Research Article

100

INDONESIAN SCHOLAR SOCIETY

Indones. J. Chem. Stud.
2026, 5(2), 100–108
Available online at journal.solusiriset.com
e-ISSN: 2830-7658; p-ISSN: 2830-778X

Indonesian Journal of Chemical Studies

Synthesis of KI/Hydroxyapatite Catalyst from Tenggiri Fish (*Scomberomorus guttatus*) Bone Waste as a Crude Palm Oil Interesterification Catalyst

Hanifa Setya Ningrum[1], Tedi Kurniadi[1]*, Mentari Zikri Anty[1], Elva Stiawan[1,2], Gunaryo[1], Amadea Kenyoning Hapsari Subiakto[1], Fikriyah Hamidah[1], Zaidan Al Fajry[1], Ardine Nismara Kusumawati[1]

[1]*Department of Chemistry, The Republic of Indonesia Defense University, Bogor 16810, Indonesia*

[2]*Leiden University, 2300 RA Leiden, The Netherlands*

Received: 14 Sep 2025; Revised: 24 Oct 2026; Accepted: 25 Oct 2026;
Published online: 24 Nov 2026; Published regularly: 30 Des 2026

Abstract— This study aims to synthesize and test the effectiveness of a hydroxyapatite (HAp) heterogeneous catalyst derived from Tenggiri fish bone waste (Scomberomorus guttatus) impregnated with Potassium Iodide (KI) as a catalyst in the crude palm oil (CPO) interesterification reaction. HAp was synthesized by the hydrothermal method and then impregnated with KI. The synthesized KI/HAp catalyst was characterized using FTIR and XRD. FTIR results show absorption bands at wavenumbers 3448, 1627, and 1041 cm ¹, indicating the presence of OH^-, CO_3^{2-}, and PO_4^{3-} groups in hydroxyapatite. The data are corroborated by the XRD results, which showed diffraction peaks at 2θ = 26.03°, 32.11°, and 32.98°, in accordance with the JCPDS reference data No. 09-0432. The effect of variation in catalyst weight concentration on CPO interesterification results was analyzed through biodiesel quality parameters, including density, viscosity, acid number, and iodine number, and further characterized using GC-MS. The best results were obtained using a KI/HAp catalyst at 2.5% (w/w), yielding 81.30% product and demonstrating optimal performance across biodiesel quality parameters. The methyl oleate compound was identified in the GC-MS analysis at a retention time of 22.693 minutes. This research demonstrates the potential of using Tenggiri fish bone waste as a raw material for environmentally friendly catalysts in CPO interesterification.

Keywords— *Biodiesel; Fish bone waste; Hydroxyapatite; Interesterification; Potassium iodide*

1. INTRODUCTION

Currently, the world's energy needs rely heavily on fossil fuels such as petroleum, coal, and natural gas. The rapid depletion of these fossil fuel reserves has led to an energy crisis and economic instability [1]. Therefore, it is crucial to identify efficient, renewable alternative fuels that are readily available, reduce dependence on non-renewable resources, and minimize pollution.

Biodiesel is a renewable fuel derived from vegetable oils, animal fats, and waste cooking oils, and is considered a more environmentally friendly alternative to petroleum-based diesel [2]. It offers several advantages, including reduced exhaust emissions, biodegradability, and compatibility with existing diesel engines [3]. However, conventional biodiesel production typically results in about 10% by-product in the form of crude glycerol [2]. As biodiesel production continues to increase, the accumulation of glycerol has become a concern due to its limited demand [4]. Glycerol is generally produced as a by-product of the transesterification reaction, which involves converting triglycerides in oils with alcohol [5].

An alternative to this method is biodiesel production via interesterification, which involves the reaction of triglycerides with carboxylic acid esters such as methyl acetate, replacing alcohol as a reactant [4]. Unlike transesterification, interesterification produces triacetin, a compound used as a fuel additive [6].

In biodiesel processing, catalysts play a crucial role in accelerating the reaction rate. Conventionally, biodiesel production utilizes homogeneous catalysts, either acidic or basic [7]. However, homogeneous catalysts have several drawbacks, including single-use application, increased costs, waste generation, and the need for complex product separation [8]. As an alternative, heterogeneous catalysts have been widely studied due to their advantages such as reusability, ease of separation from the final product, faster reaction rates, and greater cost efficiency [9].

Common heterogeneous catalysts used in interesterification reactions include metal oxides [10], mixed metal oxides [9], modified silica [11], hydrotalcites [12], ion-exchange resins [13], and immobilized lipases [14]. However, many of these catalysts require long reaction times and are costly, limiting their commercial viability.

Recently, there has been growing interest in using

***Corresponding author**.
Email address: kurniadi75@gmail.com
DOI: 10.55749/ijcs.v5i2.104

solid waste materials as low-cost precursors for the synthesis of heterogeneous catalysts. One such waste is fish bone, a by-product of the fisheries industry that is abundantly available in Indonesia [15]. Specifically, tenggiri fish bones are rich in calcium, which can be utilized to synthesize hydroxyapatite (HAp) [16]. Hydroxyapatite is a mineral primarily composed of calcium and phosphorus and has been used as a catalyst support in imine synthesis [17], CO_2 cycloaddition reactions [18], cross-coupling reactions [19], as well as esterification and transesterification processes [20]. These applications are attributed to its unique structure, high adsorption capacity, and ion-exchange ability [21]. The catalytic properties of hydroxyapatite can be enhanced through various modifications, such as impregnation with basic substances [22].

Among the most effective basic substances is potassium, known for its strong basic active sites [22]. Potassium iodide, in particular, has demonstrated high catalytic activity in biodiesel production. For example, Marinkovic et al. [23] achieved a biodiesel yield of up to 99.99% using KI/Al_2O_3; Malani et al. [24] obtained 94.71% with KI/ZnO; [25] produced 91.78% using KI/HAp derived from phosphate rock; Anbia et al. [26] yielded 87.69% with KI/eggshell; and Widayat et al. [27] reported 87.91% using KI/H-Zeolite.

However, no studies have yet explored the use of potassium iodide-impregnated hydroxyapatite derived from tenggiri fish bone waste as a heterogeneous catalyst in the interesterification of crude palm oil. Therefore, in this study, hydroxyapatite synthesized from tenggiri fish bone waste and impregnated with potassium iodide is proposed as a novel heterogeneous catalyst. It is expected that this synthesized catalyst will effectively catalyze the interesterification of crude palm oil to produce biodiesel that meets established quality standards.

2. EXPERIMENTAL SECTION

2.1. Materials

The materials used in this study include tenggiri fish bone waste, crude palm oil (CPO), and analytical-grade reagents from E. Merck, such as HNO_3, NH_3, and H_3PO_4. Other materials used include diammonium hydrogen phosphate $(NH_4)_2HPO_4$, potassium iodide (KI), bleaching earth (BE), methyl acetate, and distilled water.

2.2. Instrumentations

The instruments used in this study include Fourier Transform Infrared (FT-IR, Prestige 21), X-Ray Diffractometer (XRD MAXima-X 7000), and Gas Chromatograph–Mass Spectrometer (GC-MS Agilent 7890A).

2.3. Synthesis of Hydroxyapatite (HAp) from Tenggiri Fish Bone Waste

The synthesis of hydroxyapatite followed the procedure conducted by [28] with some modifications. The cleaned tenggiri fish bones were boiled in water for 30 minutes, then dried for 7 days. The fish bones were ground and sieved using a 100-mesh sieve, then calcined at 1000 °C for 5 hours. The calcination process produced CaO powder, which was used to prepare $Ca(OH)_2$ through a hydration reaction. A total of 25.5 g of the calcined CaO powder was dissolved in 450 mL of 2 M HNO_3. The mixture was stirred with a magnetic stirrer for 30 minutes, then filtered. The filtrate obtained was heated to 60 °C, and a 25% NH_3 solution was added until the pH reached 11, resulting in a milky white precipitate, $Ca(OH)_2$. The white precipitate was then filtered and washed with distilled water until the pH reached 7 (neutral. It was then dried in an oven at 105 °C for 3 hours to obtain $Ca(OH)_2$ powder.

Hydroxyapatite synthesis was carried out hydrothermally by mixing 20 g of $Ca(OH)_2$ and 21.3571 g of $(NH_4)_2HPO_4$ with a Ca/P ratio of 1.67/1. The mixture was then adjusted to pH 11 by adding 25% NH_3 solution. The solution was placed in a hydrothermal vessel and reacted at 140 °C for 16 hours. The resulting solid was neutralized with distilled water until the pH reached 7 and then dried at 50 °C for 3 hours to obtain hydroxyapatite powder.

2.4. Potassium Iodide (KI) Impregnation on HAp

The potassium iodide (KI) impregnation of hydroxyapatite followed the procedure reported by Widayat et al. [25]. A total of 2.5 g of solid KI was dissolved in 47.5 g of distilled water to prepare a 5% (w/w) KI solution. Then, 20 g of hydroxyapatite powder was mixed into the 5% (w/w) KI solution. The mixture was stirred and heated for 2 hours at 90 °C. The solution was filtered using filter paper, and the residue was dried at 100 °C for 3 hours to form KI/HAp powder. The KI/HAp powder was then calcined at 500 °C for 3 h [25]. The resulting catalyst was subsequently characterized using FTIR and XRD.

2.5. Degumming Bleaching of Crude Palm Oil (CPO)

The degumming and bleaching processes for CPO followed the procedure described in [29], with modifications. A total of 500 mL of CPO was added with 0.5 mL of 85% phosphoric acid. The mixture was stirred using a magnetic stirrer for 2 hours at 80 °C. After degumming, the mixture was centrifuged at 3000 rpm for 15 minutes to obtain degummed CPO.

A total of 500 mL of degummed CPO was mixed with 100 g of bleaching earth (BE). The mixture was stirred using a magnetic stirrer for 1 hour at 80 °C. After the bleaching process, the mixture was centrifuged at 3000 rpm for 15 minutes to obtain purified CPO.

2.6. Interestification of Crude Palm Oil (CPO)

The interesterification of CPO followed the procedure reported by [30], with modifications. A total of 20 g of purified CPO was placed into a three-neck flask equipped with a condenser and heated to 60 °C. Then, the KI/HAp catalyst was added at varying weight concentrations of 2%, 2.5%, and 3% relative to the weight of CPO, along with methyl acetate. The molar ratio of CPO to methyl

acetate was 1:9. The mixture was heated to a reaction temperature of 60 °C and stirred using a magnetic stirrer at 300 rpm for 3 hours. During heating, the operating temperature was monitored to ensure optimal reaction conditions.

After heating, the reaction mixture was centrifuged for 15 minutes at 3000 rpm. The filtrate obtained by centrifugation separated into three phases: the upper phase containing biodiesel, the middle phase containing triacetin and other polar compounds, and the bottom phase containing catalyst residue. The upper phase containing biodiesel was then separated, and its quality was assessed using density, viscosity, acid value, and iodine value, and it was characterized by GC-MS.

3. RESULT AND DISCUSSION

3.1. Synthesis of KI/HAp Catalyst from Tenggiri Fish Bone Waste

Tenggiri fish bone waste (*Scomberomorus guttatus*) can be utilized as a calcium source for hydroxyapatite (HAp) synthesis because HAp is obtained from the reaction between calcium and phosphate precursors. Calcium in fish bones is generally present as calcium carbonate ($CaCO_3$), so a calcination process is necessary to convert it into calcium oxide (CaO) [31]. The calcination process is carried out to remove organic components such as proteins and fats, resulting in an inorganic residue containing calcium, as described in Eq. (1) [32].

$$2CaCO_3(s) + \text{heat} \rightarrow 2CaO(s) + 2CO_2(g) \quad (1)$$

The calcium oxide (CaO) obtained from calcination of tenggiri fish bones is then converted into $Ca(OH)_2$ through a hydration process to obtain a purer compound before being used in HAp synthesis. The formation of $Ca(OH)_2$ begins by converting CaO into $Ca(NO_3)_2$ through a reaction with HNO_3 Eq. (2) [32]. This process aims to dissolve Ca^{2+} ions and remove impurities present in CaO.

$$CaO(s) + 2HNO_3(l) \rightarrow Ca(NO_3)_2(aq) + H_2O(l) \quad (2)$$

Then, the $Ca(NO_3)_2$ solution is reacted with 25% NH_3 solution until pH 11 is reached, resulting in the formation of $Ca(OH)_2$ as a white precipitate Eq. (3) [33]. The $Ca(OH)_2$ precipitate forms when the concentrations of Ca^{2+} and OH^- ions in the solution exceed the solubility product (Ksp).

$$Ca(NO_3)_2(aq) + 2NH_3(l) + 2H_2O(l) \rightarrow Ca(OH)_2(s) + 2NH_4NO_3(aq) \quad (3)$$

The calcium hydroxide ($Ca(OH)_2$) formed is then reacted with $(NH_4)_2HPO_4$ to form HAp using the hydrothermal method. The hydrothermal method is a crystallization process conducted at temperatures above room temperature (T >100 °C) using an autoclave to produce HAp in the form of single crystals or pure particles [34]. Diammonium phosphate ($(NH_4)_2HPO_4$) acts as a phosphate ion (PO_4^{3-}) source that reacts with Ca^{2+} ions from $Ca(OH)_2$ to form HAp ($Ca_{10}(PO_4)_6(OH)_2$). The compositions of $Ca(OH)_2$ and $(NH_4)_2HPO_4$ are calculated stoichiometrically to obtain a Ca/P molar ratio of 1.67/1. The formation of HAp proceeds as follows [35]:

$$10Ca(OH)_2(s) + 6(NH_4)_2HPO_4(s) \rightarrow Ca_{10}(PO_4)_6(OH)_2(s) + 12NH_4OH(aq) + 6H_2O(aq) \quad (4)$$

The formed HAp is impregnated with potassium iodide (KI) to enhance catalytic performance, allowing K^+ ions to enter the oxygen vacancies within the HAp structure. Impregnation is performed by the wet method, mixing HAp in a KI solution, then drying at 100 °C and calcining at 500 °C for 3 hours to ensure uniform distribution of K^+ ions on the catalyst surface [23]. The results of the catalyst synthesis are shown in **Fig. 1**.

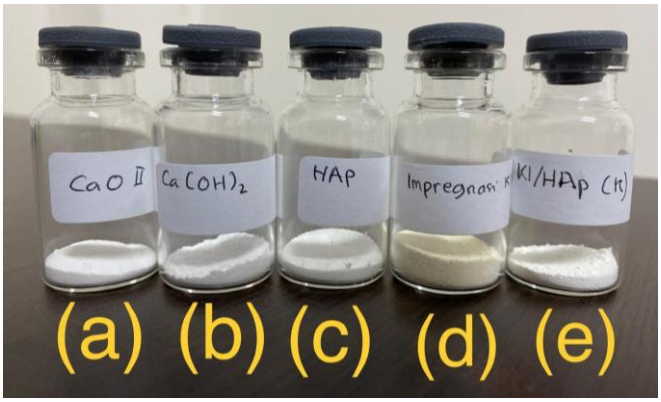


Fig. 1. (a) CaO, (b) $Ca(OH)_2$, (c) HAp, (d) KI/HAp before calcination, (e) KI/HAp after calcination

3.2. Characterization of KI/HAp Catalyst

Fig. 2 shows the FTIR spectrum of $Ca(OH)_2$, with a broad absorption band at 3425 cm^{-1}, characteristic of the stretching vibration of the -OH group. The characteristic absorption band for the C-O stretching vibration appears at 1643 cm^{-1}, and a sharp absorption band at 1381 cm^{-1} indicates the formation of $CaCO_3$ due to reaction with CO_2 in the air during preparation [36]. In the fingerprint region, the stretching vibration of P-O is observed at 1033 cm^{-1}, further confirmed by bending vibrations of P-O at 601 and 563 cm^{-1}.

The FTIR spectrum of CaO shows a characteristic absorption band at 3425 cm^{-1} from the stretching vibration of -OH, but with lower intensity compared to $Ca(OH)_2$. This indicates that part of the CaO surface has reacted with moisture in the air, forming a small amount of $Ca(OH)_2$ [37]. The C-O stretching vibration band is observed at 1627 cm^{-1}, indicating the presence of CO_3^{2-} groups from $CaCO_3$ derived from biogenic material such as fish bone [38].

In the fingerprint region, characteristic absorption bands of P-O stretching vibration appear at 1041 cm^{-1}, and are further confirmed by bending vibrations of P-O at 601 and 555 cm^{-1}. Peaks in the range of 1041–555 cm^{-1} indicate the presence of PO_4^{3-} groups resulting from the natural phosphate content in fish bone [39].

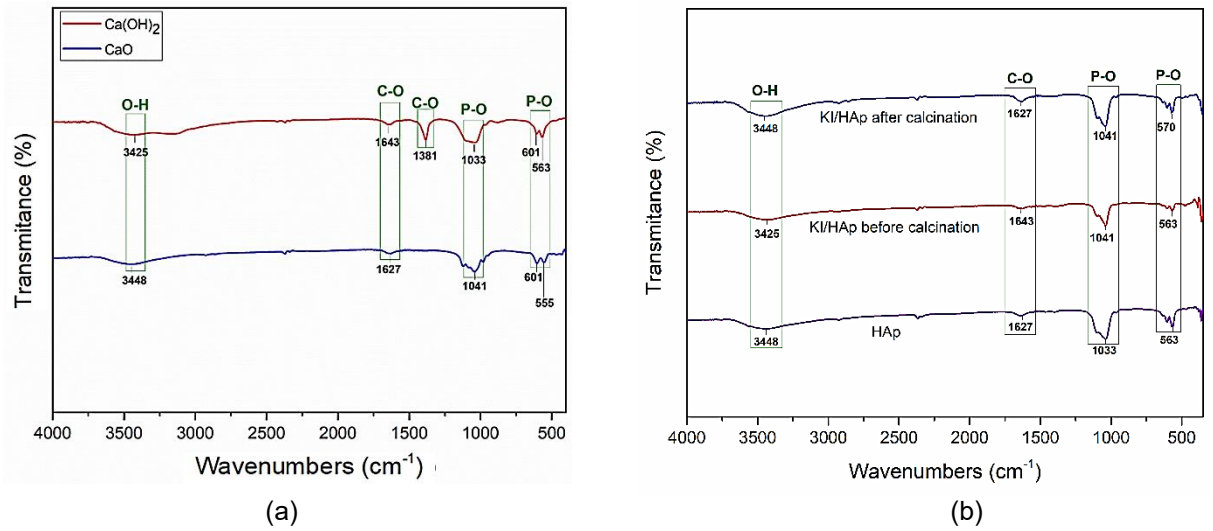


Fig. 2. (a) FTIR spectra of CaO and $Ca(OH)_2$, (b) FTIR spectra of HAp, KI/HAp before calcination, and KI/HAp after calcination

The FTIR spectrum of HAp is characterized by an absorption peak at the wavenumber 3448 cm^{-1}, which is typical of the stretching vibration of the -OH group. A characteristic absorption band for the C-O stretching vibration also appears at 1627 cm^{-1}. Additionally, a distinctive absorption band for the P-O stretching vibration is observed at 1033 cm^{-1}, further confirmed by the P-O bending vibration at 563 cm^{-1}.

The FTIR spectrum of KI/HAp before calcination shows that the absorption band of the -OH stretching vibration shifts to 3425 cm^{-1}. The C-O stretching vibration band also shifts to 1643 cm^{-1}. There is also a characteristic P-O stretching absorption peak shifted to 1041 cm^{-1}, and the P-O bending vibration appears at 563 cm^{-1} with lower intensity compared to HAp.

The FTIR spectrum of KI/HAp after calcination shows a broader absorption peak at 3448 cm^{-1} from the -OH stretching vibration compared to before calcination. The C-O stretching vibration band appears at 1627 cm^{-1}. A characteristic P-O stretching absorption peak is observed at 1041 cm^{-1}, and the P-O bending vibration shifts to 570 cm^{-1} with higher intensity compared to before calcination.

The FTIR analysis results indicate that HAp, KI/HAp before calcination, and KI/HAp after calcination share similar main functional groups, namely -OH, CO_3^{2-}, and PO_4^{3-}, which are characteristic of hydroxyapatite. This is consistent with the study by [40], which states that hydroxyapatite derived from bone generally contains the functional groups OH^-, CO_3^{2-}, and PO_4^{3-}. However, the KI impregnation process and calcination treatment cause shifts in wavenumber and changes in absorption band intensities for each functional group.

Fig 3 shows the X-ray diffraction pattern of HAp, showing sharp peaks at 2θ = 26.0264°, 32.1098°, 32.9759°, 34.1725°, 39.7787°, 46.8194°, 49.6419°, and 53.4058°, which correspond to the crystal planes (002), (211), (300), (202), (310), (222), (213), and (004), respectively. These represent the hexagonal phase of HAp, consistent with the JCPDS (Joint Committee on Powder Diffraction Standards) No. 09-0432.

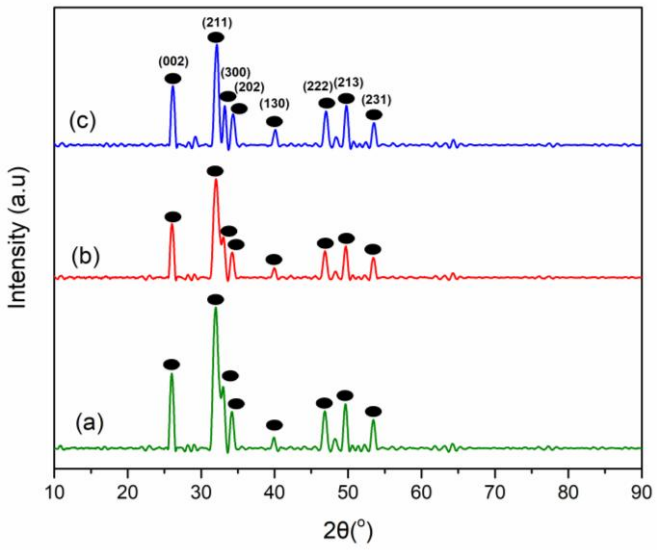


Fig. 3. XRD diffractograms of (a) HAp, (b) KI/HAp before calcination, and (c) KI/HAp after calcination

In its crystal structure, HAp is apatite-type. This crystal structure belongs to the hexagonal crystal system with the space group $P6_3/m$, characterized by lattice parameters of a = 9.36 Å and c = 6.84 Å. In this structure, Ca^{2+}, PO_4^{3-}, and OH^- ions are arranged in a regular three-dimensional pattern, which provides good crystal stability for HAp.

In line with the data, **Table 1** shows that the synthesized HAp has the highest crystallinity (70.72%) and a crystal size of 11.35 nm. The XRD diffraction pattern of KI/HAp before calcination indicates that most of the diffraction peaks of HAp experience a decrease in intensity and broadening. The decrease in intensity indicates a reduction in the degree of crystallization, while the peak broadening shows an increase in the amorphous nature of the material's structure. This corresponds to a decrease in crystallinity to 54.40% and a reduction in crystallite size to 10.50 nm. This decrease is caused by KI impregnation on the HAp surface, which

disrupts the orderliness of the HAp crystal. This indicates the formation of chemical bonds between HAp and KI, forming the KI/HAp catalyst.

Table 1. Crystallinity, crystal size, and lattice parameters of HAp, KI/HAp before calcination, and KI/HAp after calcination

Sample	Crystallinity (%)	Crystal Size (nm)	Lattice Parameter (Å)	
			a	c
HAp	70.72	11.35	9.36	6.84
KI/HAp before calcination	54.40	10.50	9.36	6.83
KI/HAp after calcination	63.14	13.05	9.32	6.80

Furthermore, the diffraction peaks of the HAp crystal at 2θ = 26.0264°, 32.1098°, 34.1725°, 39.7787°, 46.8194°, 49.6419°, and 53.4058° shift to higher angles at 2θ = 26.0586°, 32.1562°, 34.1998°, 39.8257°, 46.8422°, 49.6790°, and 53.4239°, confirming the formation of the KI/HAp catalyst structure. The crystallinity of KI/HAp before calcination is recorded at 54.40%, lower than that of HAp. The crystal size also decreases to 10.50 nm, indicating that the disruption of the HAp structure due to the addition of KI can inhibit crystal growth.

The XRD diffraction pattern of KI/HAp after calcination shows that most of the diffraction peaks of KI/HAp before calcination experienced an increase in intensity and narrowing. The increase in intensity indicates greater material crystallinity, while the peak narrowing suggests improved orderliness in the crystal structure. This aligns with an increase in crystallinity to 63.14% and significant growth in crystallite size to 13.05 nm. High-temperature calcination causes the evaporation of volatile compounds and provides additional thermal energy, allowing atoms within the crystal lattice to rearrange into a more stable and orderly configuration [41]. The diffraction peaks of KI/HAp crystals before calcination at 2θ = 26.0586°, 32.1562°, 32.9559°, 34.1998°, 39.8257°, 46.8422°, 49.6790°, and 53.4239° shift to higher angles at 2θ = 26.1700°, 32.1970°, 33.1757°, 34.3372°, 40.0323°, 46.9781°, 49.7591°, and 53.4914°, confirming the atomic rearrangement in the KI/HAp catalyst due to calcination, resulting in a denser crystal structure.

Furthermore, the diffraction peak at 2θ = 32.9759°, corresponding to the (300) crystal plane, which previously overlapped with the peak at 2θ = 32.1098°, corresponding to the (211) plane, becomes more clearly resolved after calcination. This separation indicates that calcination not only increases crystallinity but also sharpens the diffraction peaks. These changes are due to increased crystallite size and reduced strain in the crystal lattice, resulting in narrower diffraction peaks. This is consistent with decreases in the lattice parameters a from 9.36 Å to 9.32 Å and c from 6.83 Å to 6.80 Å following calcination.

Fig. 4 shows the biodiesel products resulting from the interesterification of CPO using varying catalyst weight concentrations of 2%, 2.5%, and 3%. These three variations were selected during the optimization process to identify the most effective conditions for producing high-quality biodiesel. The interesterification of CPO with varying concentrations of the KI/HAp catalyst produced clear yellowish-brown biodiesel. A noticeable difference was observed compared to the interesterification of CPO without a catalyst, which resulted in a cloudier, yellowish-brown product. This color difference is due to the inefficient progress of the interesterification reaction in the system without a catalyst, resulting in a higher content of unconverted triglycerides in the final product.

Table 2 presents test results for various product parameters obtained from the interesterification of CPO using KI/HAp catalysts at weight concentrations of 2%, 2.5%, and 3%, as well as a control sample without a catalyst. The density values for all variations were in the range of 0.9600–0.9608 g/cm³. These values are slightly higher than the SNI standard range of 0.8500–0.8900 g/cm³. A density above the standard may indicate that the interesterification reaction was incomplete, leaving behind heavier compounds such as triglycerides or diglycerides that were not fully converted into methyl esters [25].

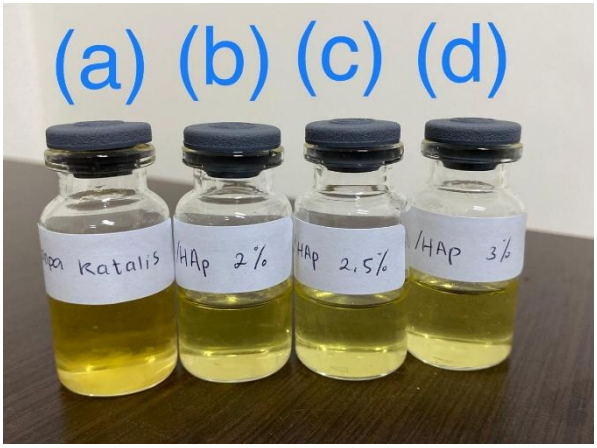


Fig. 4. Biodiesel product from CPO interesterification (a) without catalyst and with KI/HAp catalyst; weight concentrations of (b) 2%, (c) 2.5%, and (d) 3%

Table 2. Test Parameters of interesterified CPO

Sample	Density (g/cm³)	Viscosity (cSt)	Acid Value (mg KOH/g)	Iodine Value (g I_2 /100g)
Without Catalyst	0.97	1.50	2.48	48.72
KI/HAp 2%	0.96	1.70	0.62	13.28
KI/HAp 2.5%	0.96	3.15	0.56	14.14
KI/HAp 3%	0.96	3.43	0.59	16.32
SNI	0.85 – 0.89	2.30 – 6.00	max. 0.5	max. 115

The viscosity parameter increased with increasing concentrations of KI/HAp catalyst. All viscosity values were within the SNI range of 2.3–6.0 cSt, except at the 2 % concentration, which was slightly below the minimum threshold. A viscosity that is too low can lead to excessive volatility and poor lubrication, whereas a viscosity that is too high may interfere with fuel injection and combustion in engines. The increase in viscosity with higher catalyst concentrations indicates that the interesterification reaction produced more complex ester compounds, such as triesters, which have a thicker consistency.

The acid value parameter indicates the free fatty acid (FFA) content in the product. Acid values for all KI/HAp catalyst variations ranged from 0.5674–0.6277 mg-KOH/g, which exceeds the SNI maximum limit of 0.5 mg-KOH/g. High acid values can result from excessive heating of the sample, leading to hydrolysis and thus an increase in FFA content in the biodiesel [25]. High FFA levels may cause corrosion in engine combustion systems and reduce combustion efficiency due to engine fouling.

The iodine value for all variations ranged from 13.2884 to 16.3232 g I_2/100 g, which is well below the SNI maximum of 115 g I_2/100 g. A low iodine value indicates that the resulting biodiesel has a high degree of saturation. Biodiesel with high saturation typically exhibits better oxidative stability, meaning it is more resistant to degradation during storage and use. However, saturated biodiesel also tends to have a higher freezing point, which must be considered for use in low-temperature environments [29].

Table 3 shows the yield of the interesterification of CPO using KI/HAp catalyst at weight concentrations of 2%, 2.5%, and 3%. It can be observed that the yield increases with the addition of KI/HAp catalyst up to a certain concentration. In the reaction without a catalyst, the yield is only 63.20%, indicating that although the interesterification reaction can occur without a catalyst, its efficiency remains low.

The addition of 2% KI/HAp catalyst increases the yield to 73.89%. This increase demonstrates the catalyst's crucial role in accelerating the interesterification reaction by lowering the activation energy. When the catalyst concentration is increased to 2.5%, the yield rises further to 81.30%, the highest value observed in this study. This suggests that at a KI/HAp catalyst loading of 2.5%, the catalytic activity of KI/HAp reaches its optimal level.

Table 3. Comparison of interesterification yield of CPO

Sample	Yield(%)
Without Catalyst	63.20
KI/HAp 2%	73.89
KI/HAp 2.5%	81.30
KI/HAp 3%	80.06

However, when the catalyst concentration is increased to 3%, the yield slightly decreases to 80.06%. This phenomenon is caused by the saturation of active sites on the catalyst surface, which hinders the interaction between the substrate and the active sites. Additionally, excessive catalyst loading may trigger side reactions that reduce conversion efficiency [42]. These findings are consistent with the study by [43], which reported that reaction efficiency improves with catalyst addition up to an optimal concentration and tends to decline when the catalyst exceeds its saturation point.

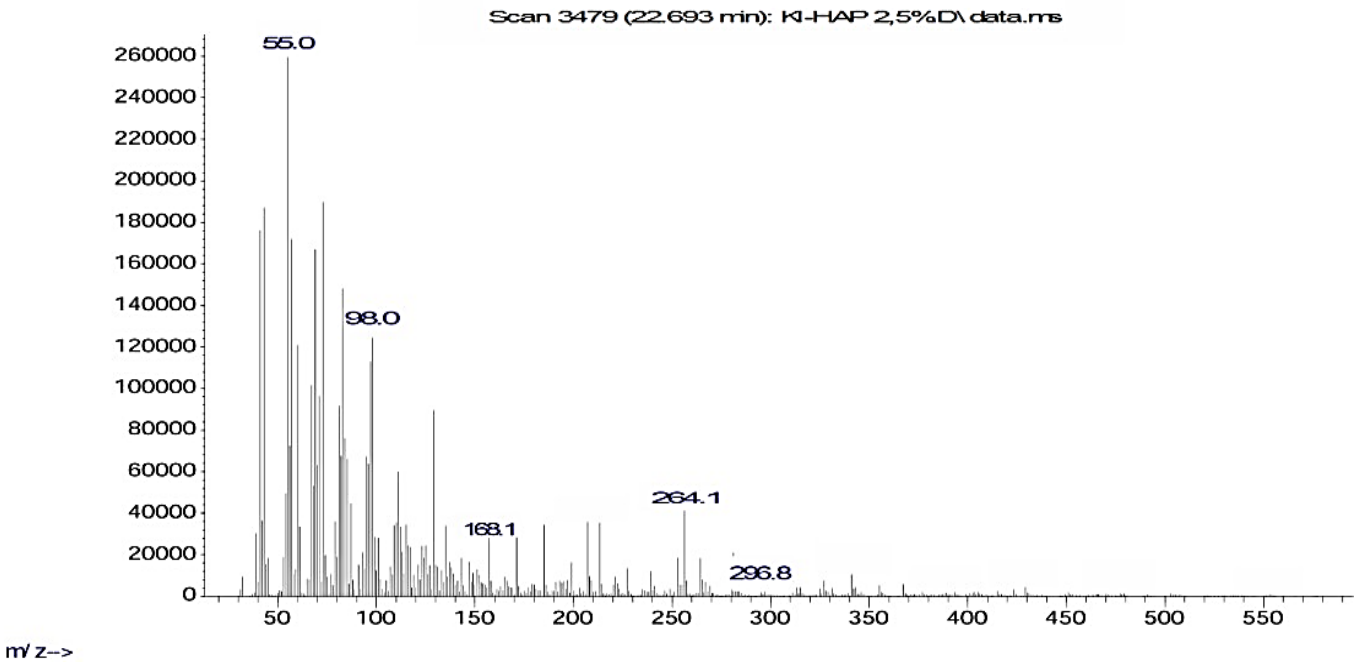


Fig. 5. Mass spectrum of methyl oleate

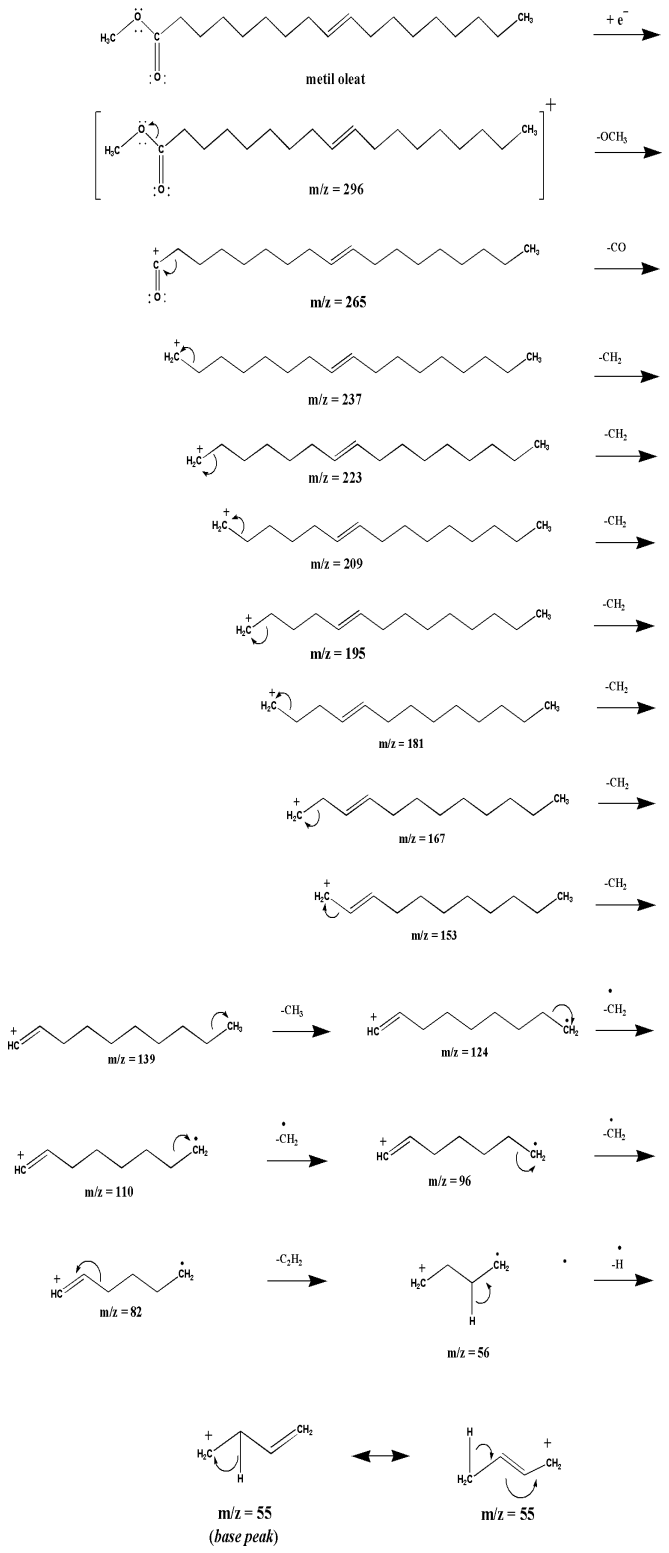


Fig. 6. Fragmentation pattern of methyl oleate

The product of the interesterification reaction of CPO using a 2.5% KI/HAp catalyst derived from tenggiri fish bone waste was analyzed using GC-MS, and the mass spectrum (**Fig. 5**) was obtained at a retention time of 22.693 minutes with an area percentage of 2.31, showing similarity to the standard compound 9-octadecenoic acid, methyl ester, (E)- (methyl oleate). **Fig. 6** shows the predicted fragmentation pattern of methyl oleate based on the resulting mass spectrum. Fragmentation occurs when chemical bonds are cleaved at specific points within the molecular structure by high-energy bombardment in the mass spectrometer, generating charged fragment ions that are detected and represented as m/z (mass-to-charge ratio) values.

The molecular ion of the compound is detected at m/z = 296, indicating the presence of the $C_{19}H_{36}O_2^+$ ion. A fragment at m/z = 265 is formed due to the loss of a methoxy group (–OCH_3) from the molecular ion. Subsequently, cleavage of the carbonyl group (–CO) from the m/z = 265 fragment results in an ion at m/z = 237. This fragment undergoes stepwise fragmentation through the successive loss of methylene groups (–CH_2), producing a series of peaks at m/z = 237, 223, 209, 195, 181, 167, 153, and 139. An ion at m/z = 124 is generated by the loss of a methyl group (–CH_3) from the m/z = 139 fragment, followed by the loss of a methylene radical (·CH_2), leading to subsequent fragments at m/z = 124, 110, 96, and 82.

The ion at m/z = 56 is formed by the loss of an ethyne molecule (C_2H_2) from the m/z = 82 ion, while the peak at m/z = 55 results from the loss of a hydrogen radical (·H) from the m/z = 56 ion. This m/z = 55 peak is known as the base peak of methyl oleate, which is relatively stable due to resonance effects.

4. CONCLUSION

Tenggiri fish (*Scomberomorus guttatus*) bone waste can be used as a calcium source for the hydrothermal synthesis of hydroxyapatite (HAp). The resulting HAp can be impregnated with potassium iodide (KI) via impregnation to form the heterogeneous catalyst KI/HAp. Characterization using FTIR and XRD showed that the synthesis and impregnation of HAp exhibited appropriate structural and functional characteristics, indicated by the presence of OH^-, CO_3^{2-}, and PO_4^{3-} functional groups, as well as diffraction peaks at 2θ = 26.0264°, 32.1098°, and 32.9759°, which correspond to the JCPDS standard No. 09-0432. The use of a 2.5% KI/HAp catalyst in the interesterification reaction of CPO resulted in an 81.30% product yield, with methyl oleate detected at a retention time of 22.693 minutes by GC-MS.

5. AUTHOR'S DECLARATION

5.1. Data Availability

There is no supporting information in this paper. The data that support the findings of this study are available on request from the corresponding author (TK).

5.2. Acknowledgments

The authors would like to express their sincere gratitude to the Republic of Indonesia Defense University for the guidance, facilities, and financial support provided through the B100 Project. We also acknowledge the Chemistry Laboratory, Unhan RI, for providing the facilities to perform this research.

5.3. Conflict of Interest

The authors declare no financial or personal conflicts of interest regarding this journal's publication.

5.4. Author Contributions

HSN, MZA, ES, Gunaryo, AKHS, FH, ZAF, and ANK performed the experiment and wrote the early manuscript. TK and MZA supervised the experiment and data calculations and revised the manuscript. TK, HSN, and Gunaryo collaborated on writing and revising the manuscript. All authors approved the final version of the manuscript.

5.5. AI Statement

ChatGPT was utilized to enhance the clarity, grammar, and overall readability of this manuscript. All technical content, data interpretation, and conclusions were solely developed and verified by the authors. The final version of the manuscript was thoroughly reviewed to ensure accuracy, coherence, and alignment with the study's findings.

5.6. Funding Statement

This research received funding from the B100 project, the Republic of Indonesia Defense University.

5.7. Ethical Clearance

Not applicable.

6. REFERENCES

[1] Muhammad, U.L., Shamsuddin, I.M., Danjuma, A., Musawa, R.U.S. and Dembo, U.H. 2018. Biofuels as the starring substitute to fossil fuels. *Pet. Sci. Eng*. 2(1). 44-49. doi: 10.11648/j.pse.20180201.17

[2] Chilakamarry, C.R., Sakinah, A.M., Zularisam, A.W. and Pandey, A. 2021. Glycerol waste to value added products and its potential applications. *Syst. Microbiol. Biomanufacturing.* 1(4). 378-396. doi: 10.1007/S43393-021-00036-W

[3] Mujeeb, M.A., Vedamurthy, A.B. and Shivasharana, C.T., 2016. Current strategies and prospects of biodiesel production: a review. *Pelagia Research Library Advances in Applied Science Research*. 7(1). 120-133.

[4] Sendzikiene, E. and Makareviciene, V. 2021. Biodiesel fuel synthesis by interesterification of triglycerides with carboxylate esters of low molecular weight. *Rev. Chem. Eng*. 37(2). 259-276. doi: 10.1515/Revce-2018-0083/Machinereadablecitation/Ris

[5] Supriadi, E., Basuki, R., Prajitno, D.H. and Mahfud, M. 2021. Produksi biofuel berbantuan ultrasonik dari minyak kelapa terkatalisis Ca/γ-Al_2O_3 dan K/γ-Al_2O_3. *Walisongo J. Chem.* 4(1). 45-56. doi: 10.21580/wjc.v4i1.7861

[6] Esan, A.O., Olabemiwo, O.M., Smith, S.M. and Ganesan, S. 2021. A concise review on alternative route of biodiesel production via interesterification of different feedstocks. *Int. J. Energy Res*. 45(9). 12614-12637. doi: 10.1002/Er.6680

[7] Shakorfow, A.M. and Mohamed, A.H. 2020. Homogenous acidic and basic catalysts in biodiesel synthesis: A review. *Acta Chem. Malaysia*. 4(2). 76-85. doi: 10.2478/Acmy-2020-0013

[8] Faruque, M.O., Razzak, S.A. and Hossain, M.M. 2020. Application of heterogeneous catalysts for biodiesel production from microalgal oil—a review. Catalysts. 10(9). 1025. doi: https://doi.org/10.3390/catal10091025.

[9] Simões, S.S., Ribeiro, J.S., Celante, D., Brondani, L.N. and Castilhos, F. 2020. Heterogeneous catalyst screening for fatty acid methyl esters production through interesterification reaction. *Renew. Energy*. 146. 719-726. doi: 10.1016/j.renene.2019.07.023.

[10] Nunes, A.L.B. and Castilhos, F.D. 2020. Chemical interesterification of soybean oil and methyl acetate to FAME using CaO as catalyst. *Fuel*. 267. 117264. doi: 10.1016/J.Fuel.2020.117264

[11] Xie, W. and Hu, L. 2016. Biguanide-functionalized mesoporous SBA-15 silica as an efficient solid catalyst for interesterification of vegetable oils. *Food Chem.* 197. 92-99. doi: 10.1016/J.Foodchem.2015.10.103

[12] Dhawan, M.S., Barton, S.C. and Yadav, G.D. 2021. Interesterification of triglycerides with methyl acetate for the co-production biodiesel and triacetin using hydrotalcite as a heterogenous base catalyst. *Catal. Today*. 375. 101-111. doi: 10.1016/J.Cattod.2020.07.056

[13] Akkarawatkhoosith, N., Kaewchada, A., Ngamcharussrivichai, C. and Jaree, A. 2020. Biodiesel production via interesterification of palm oil and ethyl acetate using ion-exchange resin in a packed-bed reactor. *BioEnergy Res.* 13(2). 542-551. doi: 10.1007/S12155-019-10051-4/Metrics S

[14] Xie, W. and Zang, X. 2016. Immobilized lipase on core–shell structured Fe_3O_4–MCM-41 nanocomposites as a magnetically recyclable biocatalyst for interesterification of soybean oil and lard. *Food Chem.* 194. 1283-1292. doi: 10.1016/J.Foodchem.2015.09.009

[15] Kusumawati, P., Triwitono, P., Anggrahini, S. and Pranoto, Y., 2022. Nano-calcium powder properties from six commercial fish bone waste in Indonesia. *Squalen Bulletin of Marine and Fisheries Postharvest and Biotechnology*. 17(1). 1-12. doi: 10.15578/Squalen.601

[16] Ng, H.M., Bee, S.T., Sin, L.T., Ratnam, C.T. and Rahmat, A.R. 2019. Effect of electron beam irradiation sterilization on biomedical polylactic acid composite filled with Scomberomorus Guttatus-derived hydroxyapatite. *Compos. Part B Eng*. 176. 107273. doi: 10.1016/J.Compositesb.2019.107273

[17] Hamidah, F., Septaningsih, D.A., Fahri, M., Basuki, R., Subiakto, A.K.H., Nismarawati, A.K., Ningrum, H.S., Al Fajry, Z., Erwinda, M.A. and Afandi, A.K. 2025. Modification of calcium oxide catalyst derived from chicken eggshell waste with magnesium oxide to enhance biodiesel synthesis from crude palm oil. *Sorpt. Stud.* 1(2). 54-59. doi: 10.55749/ss.v1i2.115

[18] Luo, D., Zhang, Z.Y., Yuan, H., Yu, X.Y., Gao, X., Hu, Z. and Chang, C.R. 2024. Ionic liquids bonded in mesoporous HAP serve as efficient catalysts for CO_2 fixation. *Chem. Eng. J*. 481. 148129. doi: 10.1016/J.Cej.2023.148129

[19] Bilakanti, V., Boosa, V., Velisoju, V.K., Gutta, N., Medak, S. and Akula, V. 2017. Role of surface basic sites in Sonogashira coupling reaction over $Ca_5(PO_4)_3OH$ supported Pd catalyst: Investigation by diffuse reflectance infrared Fourier transform spectroscopy. *J. Phys. Chem. C*. 121(40). 22191-22198. doi: 10.1021/acs.jpcc.7b07620

[20] Kalita, J., Bharali, L., Chetia, B., Chakraborty, D. and Dhar, S.S. 2024. Metal–organic framework-supported hydroxyapatite (UiO-66@HAp): an efficient catalyst for the microwave-assisted transesterification of palm oil. *Biofuels, Bioprod. Biorefining.* 18(2). 410-424. doi: 10.1002/bbb.2584

[21] Ibrahim, M., Labaki, M., Giraudon, J.M. and Lamonier, J.F. 2020. Hydroxyapatite, a multifunctional material for air, water and soil pollution control: A review. *J. Hazard. Mater*. 383. 121139. doi: 10.1016/j.jhazmat.2019.121139

[22] Chen, G., Shan, R., Shi, J., Liu, C. and Yan, B., 2015. Biodiesel production from palm oil using active and stable K-doped hydroxyapatite catalysts. *Energy Convers. Manag*. 98. 463-469. doi: 10.1016/j.enconman.2015.04.012

[23] Vasic, M., 2016. Synthesis of biodiesel from sunflower oil over potassium-loaded alumina as a heterogeneous catalyst: the effect of process parameters. *Chemical Industry*. 70(6). 639–648. doi: 10.2298/HEMIND150807001M

[24] Malani, R.S., Singh, S., Goyal, A. and Moholkar, V.S. 2017. Ultrasound-assisted biodiesel production using KI-impregnated zinc oxide (ZnO) as heterogeneous catalyst: a mechanistic approach. In *Conference Proceedings of the Second International Conference on Recent Advances in Bioenergy Research: ICRABR*. Springer Singapore. 67–81. doi: 10.1007/978-981-10-6107-3_5

[25] Widayat, W., Hadiyanto, H., Wardani, P.W.A., Az Zuhra, U. and Prameswari, J. 2020. Preparation of KI/hydroxyapatite catalyst from phosphate rocks and its application for improvement of biodiesel production. *Molecules*. 25(11). 2565. doi:

10.3390/molecules25112565
[26] Anbia, M., Masoomi, S., Sedaghat, S. and Sepehrian, M. 2019. Potassium halides-impregnated eggshell as a heterogeneous nanocatalysts for biodiesel production. *J. Environ. Treat. Tech.* 7(1). 103-108.
[27] Widayat, W., Wicaksono, A.R., Firdaus, L.H. and Okvitarini, N. 2016. Synthesis H-Zeolite catalyst by impregnation KI/KIO_3 and performance test catalyst for biodiesel production. In *IOP Conf. Ser. Mater. Sci. Eng.* 107(1). 012044. doi: 10.1088/1757-899X/107/1/012044
[28] Rahman, M., Aziz, Y. and Utama, P.S. 2021. Optimasi kondisi proses sintesis biodiesel berbasis reaksi esterifikasi palm fatty acid distillate dengan katalis Cu-hidroksiapatit dari limbah tulang ikan. *J. Bioprocess. Chem. Environ. Eng. Sci.* 2(1) .1-13. doi: 10.31258/jbchees.2.1.12-24
[29] Rahardja, I.B., Rantawi, A.B., Saputra, H. and Oktavia, D. 2023, November. The Quality control of refinery bleaching deodorize palm (RBDP) olein with variations of phosphoric acid. In *Proceedings of the 4th Borobudur International Symposium on Science and Technology 2022 (BIS-STE 2022)* (p. 398). doi: 10.2991/978-94-6463-284-2
[30] Daryono, E.D. 2020. Proses interesterifikasi minyak kelapa sawit menjadi biodiesel dengan co-solvent metil ester. *Jurnal Rekayasa Bahan Alam dan Energi Berkelanjutan*. 4(1). 1-8. doi: 10.21776/ub.rbaet.2020.004.01.01
[31] Ngatijo, N., Bemis, R., Heriyanti, H., Rahmi, R., Ulwan, N. and Basuki, R. 2021. Synthesis and characterization of nano-sized carbonated calcium hydroxyapatite (CHAp) from Rebon shrimp (*Acetes erythraeus*) as a candidate for dental restoring application. *Jurnal Kimia Valensi*. 7(2). 108-117. doi: 10.15408/jkv.v7i2.21359
[32] Putri, R., Prasojo, A.E., Lazuardy, A., Anitasari, R., Salsabila, F.A., Sasongko, N.A., Apriliyanto, Y.B., Hasibuan, A.K.H. and Ananda, D.D. 2025. Reflection loss improvement by cerium addition in chitosan-hydroxyapatite film as stealth drone candidate. *Indones. J. Chem. Stud.* 4(1). 8-13. doi: 10.55749/ijcs.v4i1.53
[33] Napoleon, S., Kuntjahjono, M.F.P., Sarweswara, W., Sasongko, N.A., Rifa'i, A., Nuha, N. and Basuki, R. 2026. Comparative heavy metal adsorption using magnetic, carbon-based, and biopolymer composite: a critical systematic review. *Sorpt. Stud.* 2(1). 20-33. doi: 10.55749/ss.v2i1.152
[34] Radulescu, D.E., Vasile, O.R., Andronescu, E. and Ficai, A. 2023. Latest research of doped hydroxyapatite for bone tissue engineering. *Int. J. Mol. Sci*. 24(17). 13157. doi: 10.3390/ijms241713157
[35] Zuliantoni, Z., Suprapto, W., Setyarini, P.H. and Gapsari, F. 2022. Extraction and characterization of snail shell waste hydroxyapatite. *Results Eng*. 14. 100390. doi: 10.1016/j.rineng.2022.100390
[36] Sinulingga, K., Sirait, M., Siregar, N. and Abdullah, H. 2021. Synthesis and characterizations of natural limestone-derived nano-hydroxyapatite (HAp): a comparison study of different metals doped HAps on antibacterial activity. *RSC Adv.* 11(26). 15896-15904. doi: 10.1039/d1ra00308a
[37] Bhattacharjee, B.N., Mishra, V.K., Rai, S.B., Parkash, O. and Kumar, D. 2019. Structure of apatite nanoparticles derived from marine animal (crab) shells: an environment-friendly and cost-effective novel approach to recycle seafood waste. *ACS Omega*. 4(7). 12753. doi: 10.1021/acsomega.9b00134
[38] Sari, M. and Yusuf, Y. 2018. Synthesis and characterization of hydroxyapatite based on green mussel shells (*Perna viridis*) with the variation of stirring time using the precipitation method. In IOP Publishing. *IOP Conf. Ser. Mater. Sci. Eng.* 432(1). 012046. doi: 10.1088/1757-899x/432/1/012046
[39] Pal, A., Paul, S., Choudhury, A.R., Balla, V.K., Das, M. and Sinha, A. 2017. Synthesis of hydroxyapatite from Lates calcarifer fish bone for biomedical applications. *Mater. Lett.* 203. 89-92. doi: 10.1016/J.Matlet.2017.05.103
[40] Cahyanto, A., Kosasih, E., Aripin, D. and Hasratiningsih, Z. 2017, February. Fabrication of hydroxyapatite from fish bones waste using reflux method. In *IOP Conf. Ser. Mat. Sci. Eng.* 172(1). 012006). doi: 10.1088/1757-899x/172/1/012006
[41] Salunkhe, P. and Kekuda, D. 2022. Effect of annealing temperature on the physical properties of NiO thin films and ITO/NiO/Al Schottky diodes. *J. Mater. Sci. Mater.* doi: 10.1007/S10854-022-08910-6
[42] Faizin, I.M., Bimantio, M.P. and Widyowanti, R.A. 2026. Application of the semi-batch method in biodiesel processing using refined bleached deodorized palm oil (RBDPO) with Variations in feed addition and temperature. *Journal of Innovation in Applied Natural Science*. 2(1).11-19. doi: 10.58723/jinas.v2i1.154
[43] Sutapa, I.W., Bandjar, A., Tehubijuluw, H., Ely, I.S., Kamari, A., Baskar, C., Sudiana, I.N. and Kadidae, L.O. 2025. Transesterification reaction on biodiesel production from bintaro oil (cerbera mangas l.) from Moluccas Island. *Int. J. Act. Mater.* 1(2). 109-118. doi: 10.62749/ijactmat.v1i2.15